Journal of Structural Geology, Vol. 9, No. 5/6, pp. 731 to 745, 1987
Printed in Great Britain

0191-8141/87 $03.00 + 0.00

Pure shear and simple shear calcite textures. Comparison of experimental, theoretical and natural data

H.-R. WENK and T. TAKESHITA

Department of Geology and Geophysics, University of California, Berkeley, CA 94720, U.S.A.

E. BECHLER

Institut Universitaire de Technologie, Troyes, France

B. G. ERSKINE

United States Geological Survey, Menlo Park, CA 94025, U.S.A.

and

S. MATTHIES

Akademie der Wissenschaften, Zentralinstitut für Kernforschung, Rossendorff 8051, Dresden, G.D.R.

(*Received* 20 *May* 1986; *accepted in revised form* 5 *March* 1987)

Abstract—The pattern of lattice preferred orientation (texture) in deformed rocks is an expression of the strain path and the acting deformation mechanisms. A first indication about the strain path is given by the symmetry of pole figures: coaxial deformation produces orthorhombic pole figures, while non-coaxial deformation yields monoclinic or triclinic pole figures. More quantitative information about the strain history can be obtained by comparing natural textures with experimental ones and with theoretical models. For this comparison, a representation in the sensitive three-dimensional orientation distribution space is extremely important and efforts are made to explain this concept. We have been investigating differences between pure shear and simple shear deformation in carbonate rocks and have found considerable agreement between textures produced in plane strain experiments and predictions based on the Taylor model. We were able to simulate the observed changes with strain history (coaxial vs non-coaxial) and the profound texture transition which occurs with increasing temperature. Two natural calcite textures were then selected which we interpreted by comparing them with the experimental and theoretical results. A marble from the Santa Rosa mylonite zone in southern California displays orthorhombic pole figures with patterns consistent with low temperature deformation in pure shear. A limestone from the Tanque Verde detachment fault in Arizona has a monoclinic fabric from which we can interpret that 60% of the deformation occurred by simple shear.

INTRODUCTION

METAMORPHIC petrologists have invested great efforts into establishing the temperature–pressure history of rocks by studying chemical reactions which are preserved in mineral assemblages. Many metamorphic processes are intimately related to deformation in the earth's crust. Equally important as pressure and temperature, and generally more difficult to establish, is the state of strain and particularly the strain path. A question which has intrigued structural geologists for a long time is whether coaxial or non-coaxial straining dominates during deformation. Arguments for or against both concepts fill the literature, dating back to the controversy between Becker (1904), who ascribed the development of schistosity to shearing, and Leith (1905), who advocated compressive thinning. Although methods of analysis have become refined, there is still wide controversy on whether highly deformed rocks such as mylonites are the result of coaxial thinning (e.g. Rehrig & Reynolds 1980, Bell 1981, Lee *et al.* 1987), or of thrusting in large-scale shear zones (e.g. Berthé *et al.* 1979, Lister & Snoke 1984, Simpson 1984, Lister *et al.* 1986) (Fig. 1).

It is generally agreed that much of the deformation of mylonites, which display strong preferred orientation of constituent minerals, is plastic (ductile) and occurs by intracrystalline slip. On the elementary scale of the crystal lattice, all deformation by slip takes place in simple shear (non-coaxial): dislocations propagate on a slip plane and displacements occur in the slip direction in increments of the Burger's vector. In general, geologists are not concerned with atomic movements within a single crystal. Even deformational variations on a larger scale due to heterogeneities in rock composition are often not relevant to establish the deformation mode of large structural units of tectonic significance. Yet it is by studying microscopic features and processes that we can gain insight into the macroscopic regime of deformation. This has been documented on the scale of the petrog-

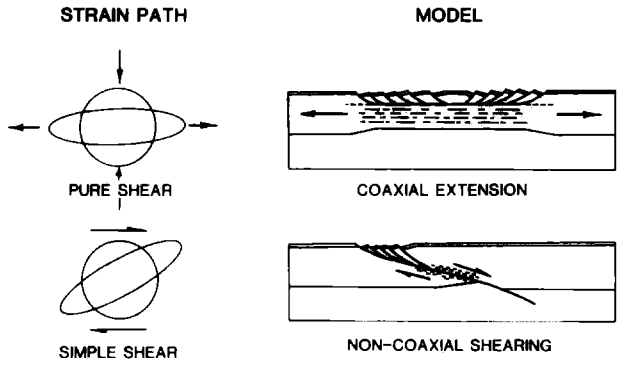

Fig. 1. Schematic diagram illustrating finite strain, coaxial and non-coaxial strain modes, and corresponding geological situations.

raphic microscope with S and C structures (Berthé *et al.* 1979) which are excellent indicators for the sense of shear.

In this paper we explore the development of lattice preferred orientations by intracrystalline slip, which is a direct result of the simple-shear deformation of component crystals. Preferred orientations not only provide information of the sense of shear but also on the relative importance of the coaxial and non-coaxial strain components. Lister & Williams (1979) and Lister & Hobbs (1980) have investigated preferred orientation in sheared quartzite. We analyze calcite polycrystals because there is a large amount of experimental data on deformation mechanisms, strength and texture development, and marbles and limestones are important components in tectonically active zones.

Our approach in this study is to first establish texture development experimentally, for various conditions. The second step is to simulate the texture evolution theoretically, using the Taylor model, and to compare simulations with experimental results. If satisfactory agreement in the orientation distributions suggests that the Taylor model is indeed applicable and that parameters such as critical resolved shear stresses and strain increments have been properly chosen, we can then proceed with making predictions for conditions for which no experimental data exist but which may be important geologically. One example is simple-shear deformation at low temperature. Finally, if there is evidence that experimental and natural specimens are deformed by similar mechanisms (e.g. dislocation microstructures, Barber & Wenk 1979), we are in a position to compare natural textures with experimental or theoretical textures of a known strain history and, if a close coincidence exists, provide an interpretation.

The use of preferred orientation data in structural geology is well established. A qualitative interpretation relating the symmetry of pole figures to the symmetry of the strain path (Paterson & Weiss 1962) is straightforward and easily visualized, but information is limited. As soon as we start to comment on changes in patterns or pole densities we find it necessary to rely on elaborate theories which are not easily accessible and require substantial investment. Many of our techniques are borrowed from metallurgical research of the last 10 years, which has lead to a revolution of 'quantitative' texture analysis. While we cannot provide an introduction of all aspects to the structural geologist, we try to elucidate some of the basic issues and refer to pertinent literature. A thorough introduction and comprehensive bibliography is provided by Wenk (1985).

We see three major sources of difficulty. The first one is texture representation. Pole figures give information on the distribution of a single crystal direction (e.g. quartz c = [0001] axes) with respect to the sample coordinates. However, to describe adequately the texture, we must relate the two co-ordinate systems, that of the crystal and that of the specimen, and this requires three angles instead of two. We will try to explain this three dimensional relationship which is called the orientation distribution function (ODF).

The second difficulty concerns the pole figure inversion needed to obtain the ODF. Some of the complexity is alluded to in several chapters of Wenk (1985), and a considerable number of definitions and constraints, including discussions of errors, are necessary for quantitative texture analysis to be meaningful. We try to reduce this discussion to a minimum and have set paragraphs containing technical details in small print.

The final difficulty lies with Taylor calculations. They need to be in five-dimensional space, which is beyond visualization. In this paper we leave out all mathematical details, and results simply have to be accepted. There is considerable literature on this subject such as the excellent monograph by Gil Sevillano *et al.* (1980).

METHODOLOGY

General comments

Ductile deformation of crystals at temperatures less than one half the melting point occurs mainly by intracrystalline slip (Frost & Ashby 1982). At higher temperatures diffusion becomes important, and other mechanisms become active. This slip on glide planes, if proper boundary conditions are imposed, causes the crystal lattice to rotate with respect to an external coordinate system. For example, if a crystal deforms by single slip (only on one slip plane and in one slip direction), a shape change is achieved without rotation if the crystal is not confined (Fig. 2a). However, if we impose external constraints such as two pistons in a compression test which keep two surfaces of the crystal parallel, there is an effective external rotation β of the crystal lattice with respect to piston axes (Fig. 2b). In a polycrystal, neighboring grains impose similar constraints, leading to changes in the orientation distribution of the crystallites.

The lattice rotations apply not only to coldworked materials but also to dislocation creep (glide plus climb) at higher temperatures or slower strain rates, a process accepted as the pervasive deformation mechanism under many geological conditions. If—at higher temperatures

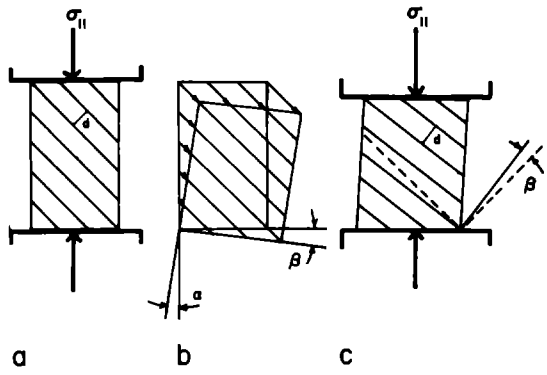

Fig. 2. During compression a rectangular crystal (a) deforms by slip into a parallelogram (b). Since pistons keep two sides of the crystal parallel, a lattice rotation, β, is imposed with reference to external co-ordinate axes (e.g. σ_{11}) (c).

and slow strain rate—dislocation glide is associated with climb, climb is generally rate controlling, but only the glide component contributes to orientation changes. In a glide and climb regime, the resulting pattern of preferred orientation is similar to that for pure glide, but for a given amount of deformation orientation densities are less pronounced. Other mechanisms, such as superplastic flow or cataclastic deformation (as long as crystals are equiaxed), do not produce preferred orientation. We will not consider recrystallization which may enforce or weaken a pre-existing deformation fabric (Gottstein & Mecking 1985). In the case of calcitic rocks, we observed that recrystallization is often outlasted by deformation which overprints the previous history.

Texture representation

Preferred orientation which develops during deformation is adequately described if we specify the relationship between external specimen co-ordinates $X^sY^sZ^s$ and the co-ordinates of the individual crystals $X^cY^cZ^c$. Three angles are required to specify an orientation relationship, and in a polycrystal we refer to such a representation as a three-dimensional orientation distribution function, or ODF.

Cartesian specimen co-ordinates are generally defined on the basis of mesoscopic fabric co-ordinates (e.g. X^s normal to the foliation or shear plane, Y^s parallel to the lineation, Z^s normal to X^s and Y^s, Y^sZ^s is the foliation plane) or with respect to strain directions (e.g. X^s parallel to the direction of shortening and Y^s parallel to the direction of elongation in a pure shear deformation experiment). Crystal co-ordinates $X^cY^cZ^c$ are assigned in concordance to symmetry elements in the crystal. We have followed the convention of Van Houtte and Wagner (1985, p. 252) in placing a Cartesian co-ordinate system in the trigonal calcite crystal (Fig. 3a) (note that this convention is different from that used by Wagner *et al.* 1981). X^c aligns with the C_2 axis of the crystal $[2\bar{1}\bar{1}0]$ and Z^c with the C_3 axis [0001]. Y^c thus falls on $[01\bar{1}0]$.

Structural geologists are more familiar with two-dimensional fabric diagrams or pole figures which display the distribution of a single crystal direction [*uvw*] (or pole to a lattice plane [*hkl*]) with respect to specimen co-ordinates. This can be done with two angles, a pole distance (or co-latitude) and a rotation (or longitude). However, a pole figure description is incomplete. From a [0001] pole figure it is impossible to infer the *a* axes or $\langle 2\bar{1}\bar{1}0\rangle$ distribution, and from a $\langle 2\bar{1}\bar{1}0\rangle$ pole figure it is difficult to estimate the *c* axes or [0001] distribution. Therefore pole figures are difficult to visualize and to interpret. It would be preferable to have a representation in which a density can be associated immediately with full orientation information, as is the case for an ODF.

The orientation distribution has been most often represented as a three-dimensional density function of Euler angles $\Psi\Theta\Phi$ (Roe 1965; note the transformation to the Bunge 1965, convention: $\Psi = \phi_1 - 90°$; $\Theta = \Phi$, $\Phi = \phi_2 + 90°$). We will plot this function in spherical co-ordinates as *partial* [0001] *pole figures which represent sections of the crystal orientation distribution* (COD) (Wenk *et al.* 1985; Wenk & Kocks 1987). Since this is new and, in our view, advantageous, we find a more elaborate description necessary. We assume that the reader is familiar with fabric diagrams.

Wenk & Kocks (1987) have used the image of sailboats on the ocean. In order to have good information on the navigational activity we wish to know for each sector on the earth the number of sailboats and the direction in which each one is heading (Fig. 4a). Two geographic co-ordinates (Ψ, Θ) define the location of the boat on the earth, and an azimuthal angle, Φ defines the direction in

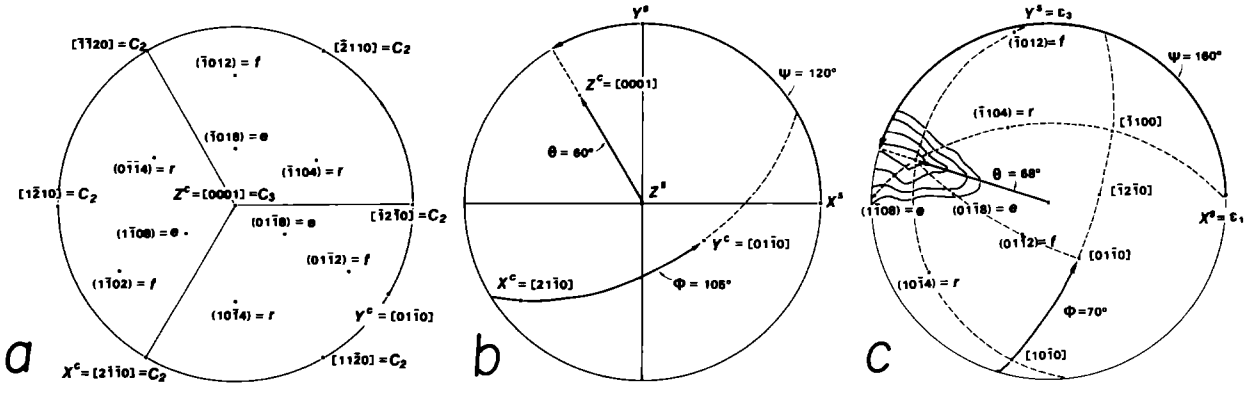

Fig. 3. Definition of co-ordinate systems. (a) Rectangular co-ordinate system $X^cY^cZ^c$ placed in the calcite crystal. (b) Definition of Euler angles Ψ, Θ, Φ which relate the co-ordinate systems $X^cY^cZ^c$ and $X^sY^sZ^s$. (c) Geometric interpretation of an orientation maximum in a partial pole figure (Φ = 70° section from Fig. 7). The full crystal orientation can be derived with an equal-area net.

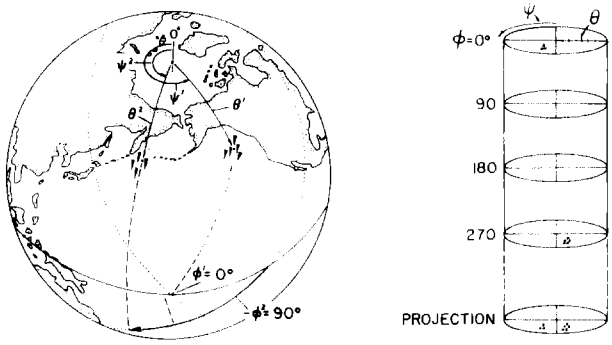

Fig. 4. Distribution of eight ships (arrows on the surface of the earth). There is a cluster of three and a cluster of five ships which head in different directions and are thus represented in different Φ sections of the orientation cylinder. A projection of the Φ sections gives a distribution of all ships irrespective of their heading. Corresponding angles Ψ, Θ, Φ are indicated.

which the boat is heading. We represent and classify now in a $\Phi = 0°$ partial pole figure the locations of all those boats which are heading towards the point where the great circle around the boat position intersects the equatorial plane ($\pm \Delta$ degrees); in a $\Phi = 10°$ partial pole figure the density of those boats heading $10° \pm \Delta$ off that point on the equator; and so on (Fig. 4b). A complete set of partial pole figures contains the full information about directions and locations of boats. The finer we choose our interval in Φ, the higher is the resolution of our representation.

By analogy, crystals could be viewed as having a mast, the Z^c = [0001] axis, and a heading, the Y^c = [01$\bar{1}$0] direction. If we know the Z^c axis ('location') and the Y^c axis ('direction'), we know the full orientation of a crystal. Assume a certain Z^c direction specified by two angles, $\Psi = 120°$ and $\Theta = 60°$ (Fig. 3b). The X^c and Y^c axes of that crystal lie somewhere on a great circle about Z^c (dashed). We specify the location of Y^c by a third azimuthal angle, $\Phi = 105°$, measured counterclockwise away from the equatorial plane X^sY^s. In a partial pole figure we collect and display the distribution of only those Z^c axes which have a particular value of Φ. By contrast, a normal Z^c = [0001] pole figure displays the distribution of all [0001] axes, but does not contain any information about Y^c = [01$\bar{1}$0] axes.

In practice we normalize the distribution of individual orientations and express them as densities per unit volume such that the integral over all locations (ΨΘ) and all directions (Φ) is unity, and contour in the Φ cylinder (Fig. 4b) surfaces of equal density. Since paper is two-dimensional, we represent the three-dimensional distribution as a finite series of two-dimensional sections, the partial pole figures.

An average of densities (or summation in the case of individual orientations) over all partial pole figures yields a [0001] pole figure which contains all [0001] axes irrespective of their Y^c = [01$\bar{1}$0] orientation. This average can also be viewed as a projection along the cylinder axis Φ. Because of superpositions, projections are always smoother than the true distribution, and information is lost, as is evident by comparing the bottom diagrams in Fig. 7 and 8 with the CODs above.

How can we geometrically interpret density variations in the COD and determine the full crystal orientation which corresponds to a certain maximum in the COD? Take, for example, the concentration at $\Psi = 160°$, $\Theta = 68°$ in a $\Phi = 70°$ section of an experimentally deformed specimen (c.f. Fig. 7). The [01$\bar{1}$0] axis for the [0001] axis at $\Psi = 160°$, $\Theta = 68°$ lies on a great circle 70° off the equator (Fig. 4c). With an equal area net we can readily construct the complete orientation (dashed lines in Fig. 4c), something which cannot be done from an ordinary pole figure. We notice, for example, that for this orientation the compression direction X^c is nearly normal to an e = (1$\bar{1}$08) plane and the extension direction Y^s is nearly normal to a f = ($\bar{1}$012) plane. Such a coincidence of certain crystal and sample directions is, however, purely geometrical and can be used to describe texture components. It does not allow an immediate physical interpretation about deformation mechanisms such as that the slip plane normal should be parallel to the compression axis, as may be the case if a single crystal deformed by single slip and were not confined by neighbors. It should be understood that the COD is a comprehensive method for representing and visualizing an orientation distribution. It is not a means for interpreting textures. The latter can be approached with model calculations such as the Taylor theory.

Note that partial pole figures for calcite have only to extend from $\Theta = 0°$ to 120° due to the trigonal crystal symmetry, i.e. [01$\bar{1}$0], [$\bar{1}$010] and [1$\bar{1}$00] are equivalent (Fig. 3a). Also, specimen symmetry is expressed in the COD. A two-fold axis in Z^s is immediately visible (c.f. Fig. 7 for orthorhombic and Fig. 8 for and monoclinic symmetry). A two-fold rotation in X^s (orthorhombic specimen) in combination with a two-fold rotation in X^c (symmetry of calcite with C_2 in [11$\bar{2}$0]) (Fig. 3a) produces an equivalence of angles Ψ, Θ, Φ and 180 − Ψ, Θ, 180 − Φ, respectively, 180 − Ψ, Θ, 60° − Φ (Helming and Matthies, 1984). This means that for orthorhombic specimens we only need Φ sections from 30 to 90° (only those are reproduced in the pure shear CODs of Fig. 7; note that sections from 0 to 60° do not provide sufficient information). The three angles, Ψ, Θ, Φ of the COD (longitude, latitude and azimuth) are identical to the Euler angles of the ODF which are three rotations to bring the crystal co-ordinate system $X^cY^cZ^c$ to coincidence with the specimen co-ordinate system $X^sY^sZ^s$ (Bunge 1965, Roe 1965). The partial [0001] pole figures (COD) are just a different way of looking at Φ-sections of an ODF which we find much easier to visualize and to interpret than the traditional Cartesian representations.

Textures in this paper are represented as selected (0006) and (11$\bar{2}$0) pole figures (Figs. 5 and 6) and as partial pole figures (CODs) (Figs. 7 and 8). Note that by convention, the origin of Ψ in partial pole figures is by definition in the E point (Figs. 7 and 8). Therefore, [0001] pole figures which are projections of the COD (bottom row of Figs. 7 and 8) are rotated 90° clockwise relative to measured pole figures which are shown with horizontal foliation plane (Fig. 5).

Pole figures of experimental and natural samples (Figs. 5 and 6) were measured by X-ray and neutron diffraction. In the case of X-rays, pole figures are incomplete, due to a defocusing effect which adds some uncertainty at high angles. In addition, the c-axis pole figures of calcite that geologists are most familiar with are difficult to measure with X-ray techniques because the (0006) reflection is very weak and close to the strong (10$\bar{1}$4) reflection. We have added the (0006) pole figures in Fig. 5 for reference but have not used them in the ODF calculations. Similarly with neutrons, (11$\bar{2}$0) and (20$\bar{2}$2) are very weak whereas (0006) is strong, and again we selected those which are most reliable. The COD of these samples has then been obtained by deconvolution of three to five pole figures using the method WIMV (Matthies & Vinel 1982) for triclinic specimen symmetry and trigonal crystal symmetry. The near orthorhombic or monoclinic specimen symmetry expressed in the CODs is not implied in the pole figure inversion, but results from the actual symmetry of the deformation process. We have previously applied the harmonic method and obtained ODFs from five pole

Table 1. Specifications for samples, pole figure measurements and ODF calculation

Sample	Pole Figures Used (N = neutron, X = X-ray	WIMV-ODF Minimum m.r.d.	Maximum	Average error R
K 373, 100°C pure shear	X110, X104, X202	0.29	4.72	4.85%
K 338, 300°C pure shear	N006, N104, N012, N113	0.30	3.26	4.06%
K 371, 400°C simple shear	N006, N012, N113, N104	0.21	5.79	3.17%
OS21 Palm Canyon	X110, X104, X202	0.17	6.51	4.56%
TV1 Tanque Verde	X110, X104, X202	0.44	2.14	7.22%

figures (Wagner *et al.* 1984), but we found that results with WIMV—while qualitatively similar—are more consistent, and agreement between observed and recalculated pole figures is much better. Table 1 gives information about the pole figure selection and also shows average errors between observed and recalculated pole figures. This error reflects the quality of the measured data used in the calculations. Pole figures and the CODs of theoretical predictions were calculated by expanding 5760 individual orientations with spherical harmonics to order $l = 16$ using even and odd functions (Wagner *et al.* 1981).

EXPERIMENTS

Most deformation experiments on minerals have been performed in axial compression. Only a few plane strain experiments have been conducted which allow us to address the problem of distinguishing between pure and simple shear. In this comparative study we rely on experiments on fine-grained limestone discussed by Wenk *et al.* (1981) and Wagner *et al.* (1982) for pure shear and by Kern & Wenk (1983) for simple shear and refer the reader to the original papers for experimental details. In these experiments grains became flattened and distinct preferred orientation patterns developed at about 10% strain (Wenk *et al.* 1981). Preferred orientation increased with further straining, and we illustrate textures of samples which have been shortened 30–40%. There is no optical or TEM evidence for recrystallization in any of the samples. Pole figures are displayed with the direction of no deformation (ε_2) in the center of the pole figure (Figs. 5 and 6). Pole figures (Figs. 5 and 6) and CODs (Figs. 7 and 8) document a texture transformation between 200 and 300°C (at 10^{-4}–$10^{-6}s^{-1}$) which we

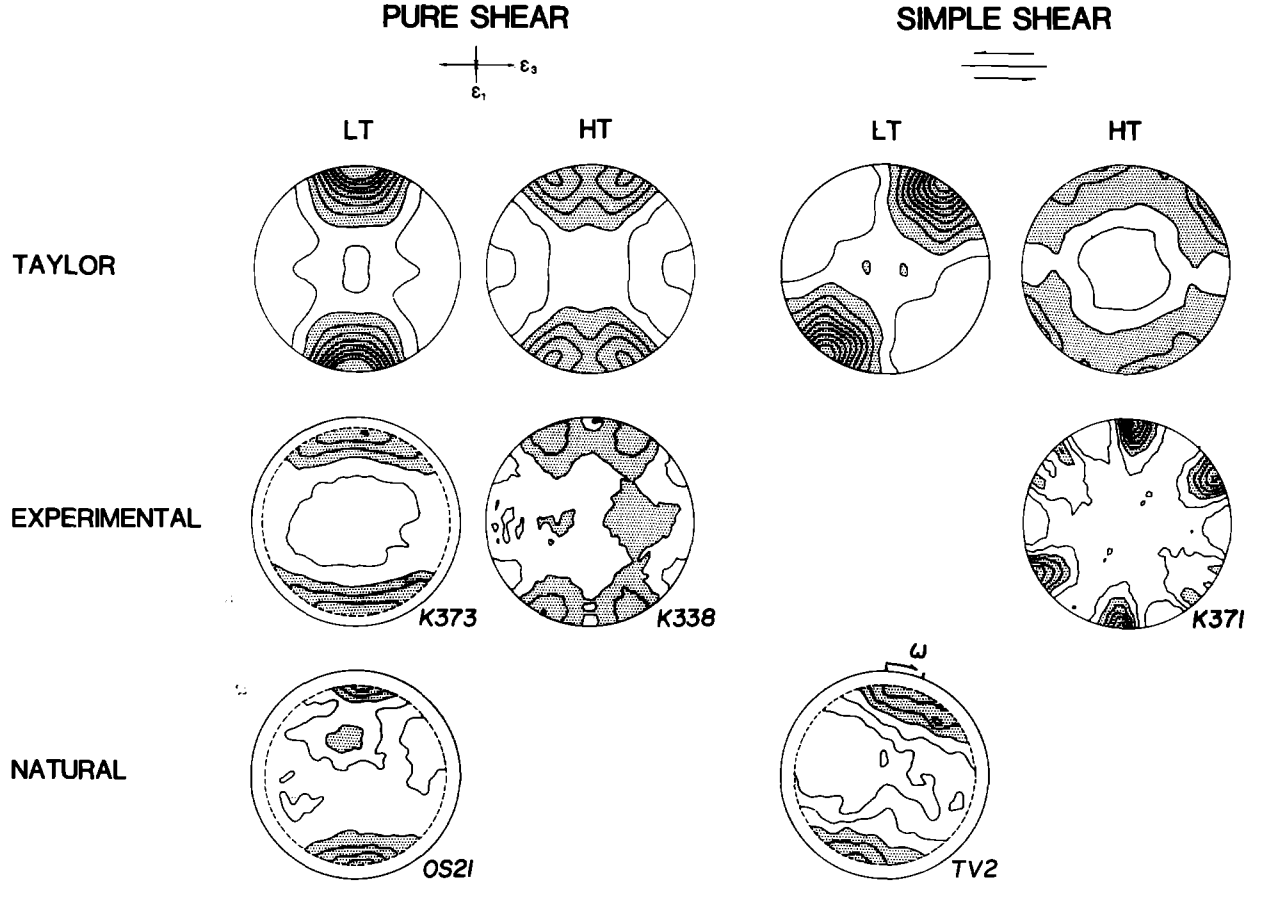

Fig. 5. c = [0001] pole figures of carbonate polycrystals. Those for experimental and natural samples are direct measurements. Complete pole figures have been measured by neutron, incomplete ones by X-ray diffraction. Equal-area projection. Contour interval for all is 0.5 m.r.d. except for TV2, where it is 0.1 m.r.d. Lowest contour is 0.5 m.r.d. shaded above 1 m.d.r.

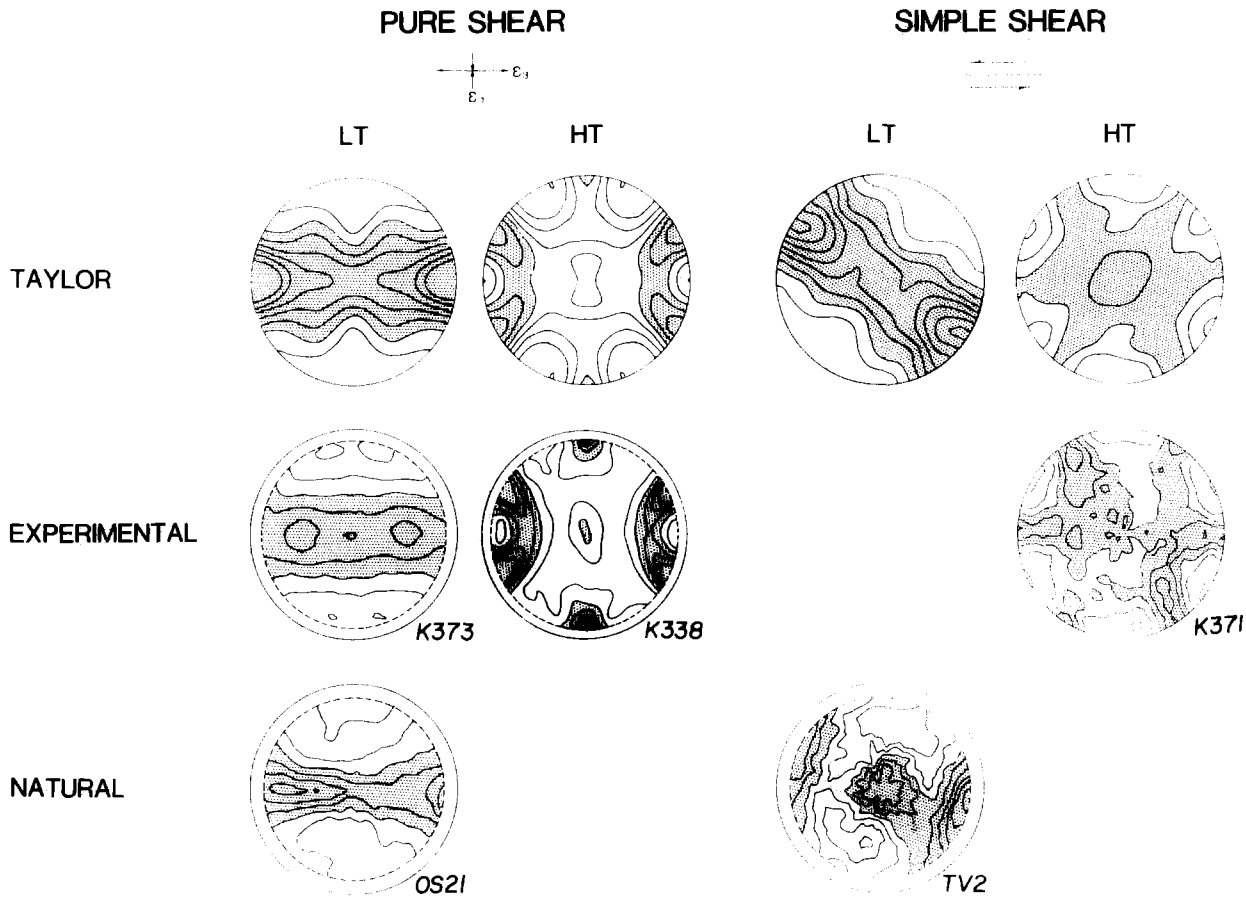

Fig. 6. $a = \langle 2\bar{1}\bar{1}0 \rangle$ pole figures of carbonate polycrystals. Same specifications as for Fig. 4 except that contour intervals are 0.25 m.r.d. shaded above 1 m.r.d.

associate with changes in the critical resolved shear stress of active slip systems. Corresponding textures will be referred to as LT (low temperature) and HT (high temperature) in the subsequent discussion. We have explored temperature as the most important variable. Clearly, strain rate should also be considered. It is generally thought to have an inverse effect on textures (Tullis *et al.* 1973). Furthermore, pressure and grain size may influence active mechanisms, particularly twinning, but data are insufficient to include these variables in our discussion.

For pure shear, pole figures (Fig. 5) and CODs (Fig. 7) are orthorhombic. Note that the two-fold axis Z^s in all experimental partial pole figures is not perfect but closely approached; in addition, sections at $\Phi = 30°$ and $\Phi = 90°$ show mirror planes. As mentioned above, Φ-sections 0–30° and 90–120° are symmetrically related to those from 30–90° and are not shown. At low temperatures, *c*-axes are concentrated in a broad maximum parallel to the direction of principal compression. At higher temperature this maximum splits into two maxima displaced about 30° towards the extension direction. The low temperature (LT) partial pole figures all have some similarity and do not change much as a function of Φ (Fig. 7, second column), indicating that *a*-axes of crystals have considerable rotational degree of freedom about their *c*-axes. This is not the case for high temperature (HT), where each partial pole figure is distinct (Fig. 7, right column). The main maximum is in the $\Phi = 70°$ section at $\Psi = 160°$ and $\Theta = 90°$ and extends through several Φ sections. The second feature is a cross ($\Phi = 30°$ section) which rotates slightly with increasing Φ and displaces maxima on it towards higher Θ angles.

So far, experimental deformation in simple shear at low temperatures has not been successful in the apparatus used by Kern & Wenk (1983). Brittle failure occurs and no ductile shear bands develop. At higher temperature, good textures develop. The symmetry is monoclinic, with only a single two-fold axis Z^s. The [0001] pole figure (Fig. 6) resembles a pure shear HT pole figure rotated by the shear angle (Kern & Wenk 1983). However, when comparing the HT COD for pure shear and simple shear (right columns in Figs. 7 and 8), it is clear that this analogy is only superficial (in these representations we assume that the shear plane is normal to X^s). For the same finite strain the simple shear texture is much stronger; furthermore, most maxima are at $\Theta = 90°$, and the cross-like component is nearly absent.

SIMULATIONS

In the previous sections we have learned how to use the COD to describe textures and how to read these diagrams to obtain information about the crystal orientation distribution. We have then documented that in

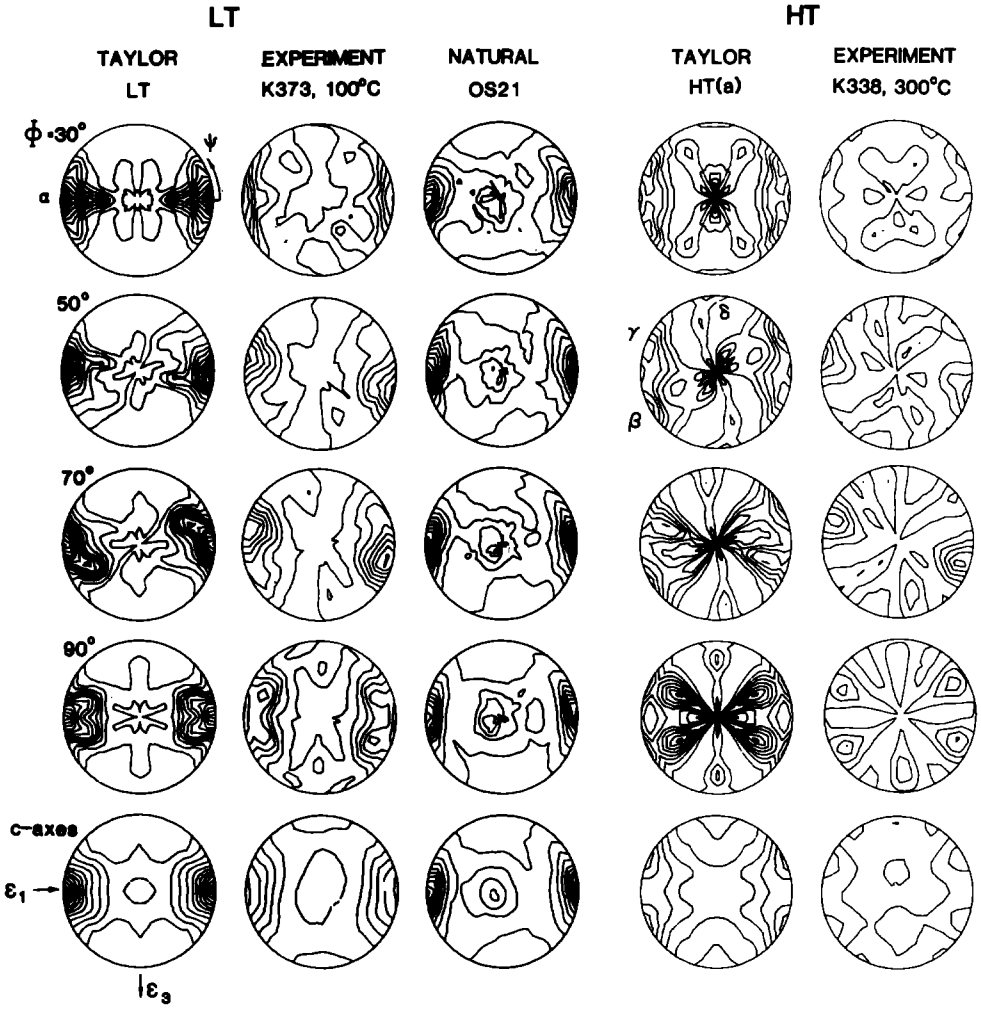

Fig. 7. Partial [0001] pole figures (CODs) in Roe (1965) co-ordinates for calcite polycrystals deformed in pure shear. Equal-area projection. Contour intervals are 0.5 m.r.d.; minimum contour is 0.5 m.r.d. Texture components $\alpha, \beta, \gamma, \delta$ are indicated. The bottom diagrams are Φ projections and represent [0001] pole figures.

experimentally deformed limestone, preferred orientations develop and patterns change as a function of temperature and strain. The next problem is to interpret the COD in terms of physical deformation mechanisms. One error that has occurred is to intuitively associate an orientation maximum with a specific slip system $(hkl)[uvw]$. Given the complex constraints and processes during polycrystal deformation, such a direct interpretation is oversimplified and lacks physical justification, as has also been pointed out by Lister & Hobbs (1980) and Gil Sevillano *et al.* (1980). For example, face-centred cubic metals deformed by {111} slip do not show a {111} maximum near the compression direction and calcite deformed by $r = \{10\bar{1}4\}$ slip and $e = \{01\bar{1}8\}$ twinning has no concentration of compression directions at either of these orientations. As in many other fields of science there are two levels of interpretation: one is pattern recognition; another explains patterns in terms of physical processes. The COD is used to represent texture data in a similar way as a ternary diagram serves to display geochemical data. In order to interpret a ternary diagram, (e.g. in terms of a crystallization sequence in igneous rocks) we have to compare the observations with either a theoretical model or experimental results.

We have used the Taylor theory to model texture development; it applies to homogeneous deformation of polycrystals by slip and mechanical twinning. The basic principles of the Taylor model as applied to calcite have been described by Lister (1978), Wagner *et al.* (1982), Van Houtte & Wagner (1985), and Wenk *et al.* (1986a). Five independent slip systems are necessary to deform a crystal in a general orientation to an arbitrary shape prescribed by the strain tensor. Of all potential slip systems, the combination of those five is chosen that requires the least amount of work. Knowing the activity on each system, we can then calculate for every crystal an effective internal rotation (Fig. 2) for a given strain increment. As the critical resolved shear stresses (c.r.s.s.) of slip systems change (e.g. with increasing temperature), different slip systems become active and crystals undergo different rotations.

We can best understand important texture transitions such as LT–HT of calcite by analyzing the topology of the single crystal yield surface (SCYS) (Lister 1978, Takeshita *et al.* 1987). The yield surface represents the yielding condition in five-dimensional stress space. Each slip plane is represented in this space by a hyperplane whose distance from the origin is the c.r.s.s. The inner

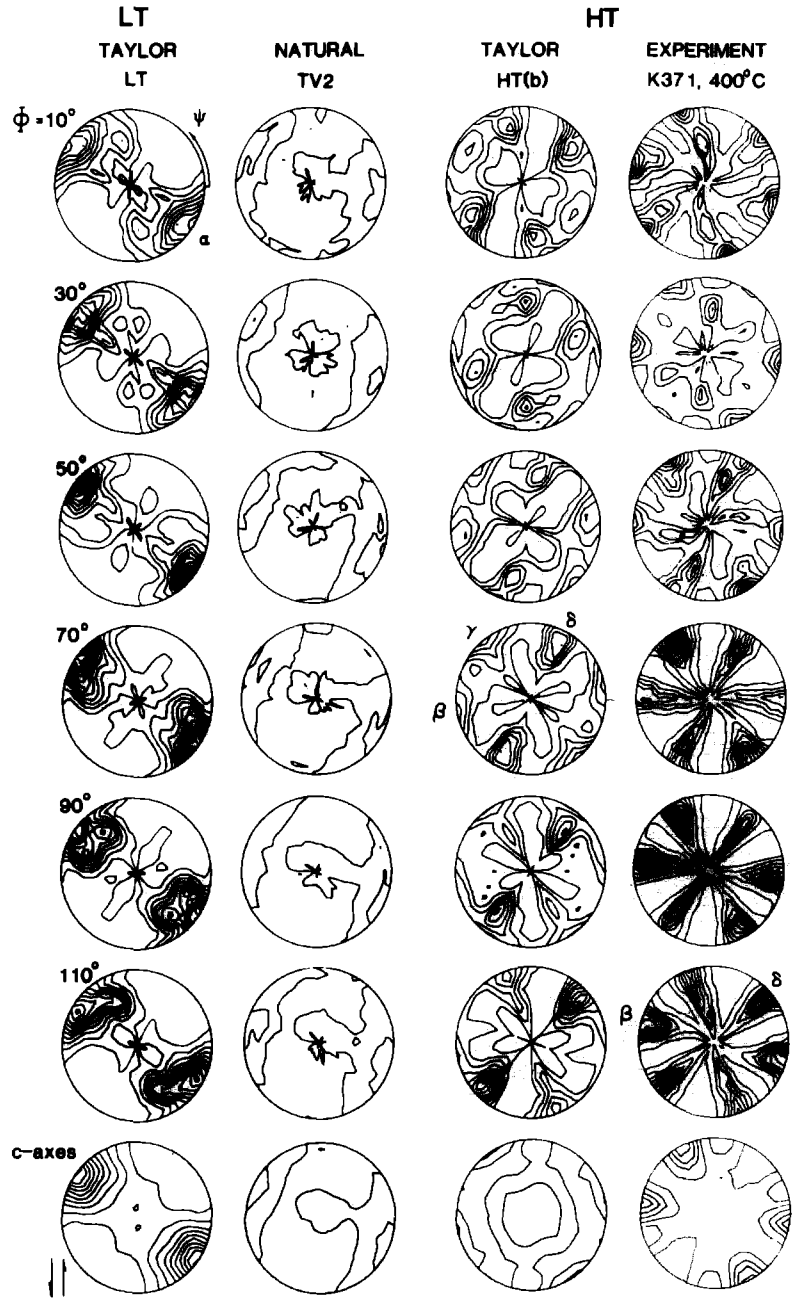

Fig. 8. Partial [0001] pole figures (CODs) in Roe (1965) co-ordinates for calcite polycrystals deformed in simple shear. Equal-area projection. Contour intervals are 0.5 m.r.d.; minimum contour is 0.5 m.r.d. Bottom diagrams are [0001] pole figures.

envelope of these hyperplanes is the SCYS. When a stress vector reaches this surface, yielding occurs. A two-dimensional analogy is illustrated in Fig. 9. The yield surface in Fig. 9(a) consists of four active slip systems and has four vertices. At each vertex, possible strain states are contained within a cone of normals. In order to satisfy any arbitrary state of strain, the yield surface needs to be closed. Slip in the positive and in the negative sense (e.g. s_1^+, s_1^-) may have different c.r.s.s., resulting in a different distance of the hyperplane from the origin. Mechanical twinning can only operate in one sense.

Modifications of the SCYS occur when the relative strengths (c.r.s.s.) of slip systems change. A slip system s_3^+ lies in Fig. 9(a) outside the SCYS and is not activated. In the case of Fig. 9(b), the hyperplane s_3^+ has intersected vertex V_1 and created two new vertices, V_1^A and V_1^B. The topologies (or surface geometries) of the two SCYSs are different, resulting in activity of different slip systems and thus producing different textures. In order to calculate the SCYS, and for Taylor texture simulations, it is necessary to know all potential slip and twinning systems and their c.r.s.s. Whereas most agree that *e* twinning and *r* and *f* slip are the dominant systems at all temperatures, there is still considerable uncertainty about the exact values of c.r.s.s. at given conditions. We rely on experimental single crystal data as much as possible (see Table 2 and Wenk 1985, table 1, p. 363 for references). But to be more confident in the applicability of the simulations it was necessary to explore systematically the influence

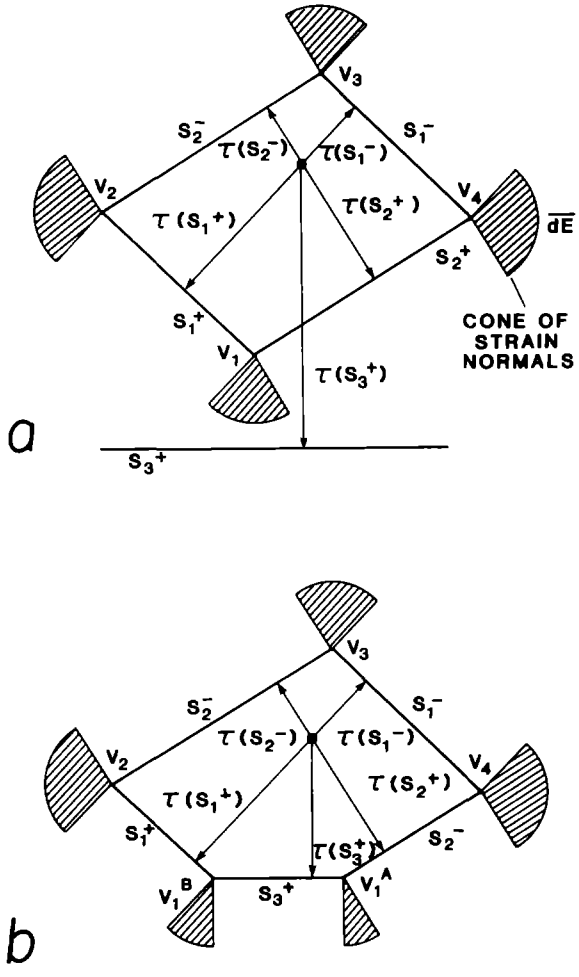

Fig. 9. Schematic sketch of a two-dimensional single crystal yield surface. (a) Slip systems s_1^+, s_1^-, s_2^+, s_2^- are active, resulting in four vertices. (b) τ_c of system s_3^+ is reduced, destroying vertex V_1 and creating new vertices V_1^A and V_1^B, resulting in five vertices. The cone of strain normals associated with each vertex is shaded.

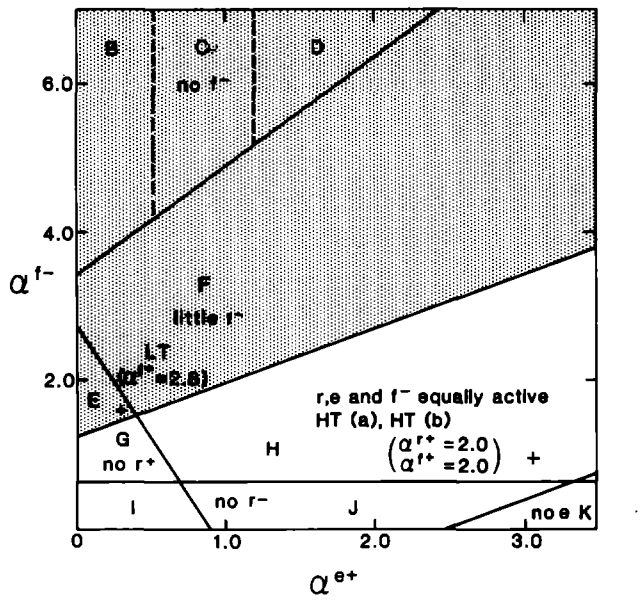

Fig. 10. Simplified topology diagram for the SCYS of calcite. Main activities of slip systems are indicated and c.r.s.s. assumptions used in this paper for LT, HT(a) and HT(b) simulations (from Takeshita *et al.* 1987). c.r.s.s. are normalized to $r^- = 1.0$. The co-ordinates are $\alpha f^- = \tau_c(f^-)/\tau_c(r^-)$ and $\alpha e^+ = \tau_c(e^+)\tau_c(r^-)$. The normalized c.r.s.s. of $\alpha r^+ = 1.5$ for all simulations. Major topologic domains are indicated and labelled (B, C, D, E, F, G, I, J and K). The LT field in which textures are almost identical is shaded. Most natural calcite textures reported so far seem to have developed in this field.

of c.r.s.s. variations on the SCYS and on texture development. This can be achieved with a topology study (Lister 1978, Takeshita *et al.* 1987). In this we assume that *e*, *r* and *f* systems are potentially active and explore the range within which c.r.s.s. can be varied without causing a major change in the combined activated slip systems. Figure 10 illustrates a simplified topology diagram for e^+, r^-, r^+ and f^- systems. We plot it in a two-dimensional space of c.r.s.s. for f^- and e^+, normalized to r^- and for a fixed α^{r^+}. In each of the fields separated by straight lines the topology of the SCYS is the same; i.e. it has the same corners, edges and faces, and therefore the same combination of slip systems are active. (This is not quite true because this simplified diagram only shows divisions with major changes. A detailed topology diagram is shown by Takeshita *et al.* 1987.) Particularly in the large shaded area where *r* and *e* dominate, simulated textures are almost identical. In this field the c.r.s.s. values correspond to those observed in single crystals at low temperature and textures compare with the LT experimental textures (see next section). Crossing from the shaded into the white area the active mechanisms change drastically. One r^- or one e^+ system is replaced by one f^- system (Takeshita *et al.* 1987, table 4). With *r*, *e* and f^- equally active, textures are much more complex and correspond to HT experimental textures. Based on single crystal data and on

Table 2. Normalized critical shear stresses for model calcite polycrystals

Glide system	Number of equivalent systems	Symbol	$\alpha = \tau^x/\tau^{r^-}$ LT	HT(a)	HT(b)
Slip					
$\{10\bar{1}4\}\langle\bar{2}021\rangle$*	3	r^+	1.6	1.5	2.0
$\{10\bar{1}4\}\langle\bar{2}02\bar{1}\rangle$	3	r^-	1.0	1.0	1.0
$\{\bar{1}012\}\langle02\bar{2}1\rangle\langle2\bar{2}01\rangle$	6	f^+	2.8	∞	2.0
$\{\bar{1}012\}\langle0\bar{2}2\bar{1}\rangle\langle\bar{2}201\rangle$	6	f^-	1.6	1.0	1.0
Twinning					
$\{\bar{1}018\}\langle40\bar{4}1\rangle$	3	e^+	0.4	3.0	3.0

* All indices refer to the $c = 17$ Å hexagonal unit cell.

Table 3. Displacement gradient tensors used in the Taylor simulations of this study. Zero components in the plane of no deformation are omitted. Ten incremental steps are applied

Pure Shear	Simple Shear
$\begin{pmatrix} -0.05 & 0 \\ 0 & 0.05 \end{pmatrix}$	$\begin{pmatrix} 0 & 0 \\ 0.1 & 0 \end{pmatrix}$

Pure shear/simple shear combined

25% Simple Shear	50% Simple Shear	75% Simple Shear
$\begin{pmatrix} -0.0475 & 0 \\ 0.0317 & 0.0475 \end{pmatrix}$	$\begin{pmatrix} -0.036 & 0 \\ 0.072 & 0.036 \end{pmatrix}$	$\begin{pmatrix} -0.0158 & 0 \\ 0.0904 & 0.0158 \end{pmatrix}$

Pure shear followed by simple shear

Simple Shear Parallel to the Foliation	Simple Shear Diagonal to the Foliation
$\begin{pmatrix} -0.05 & 0 \\ 0 & 0.05 \end{pmatrix} + \begin{pmatrix} 0 & 0 \\ 0.1 & 0 \end{pmatrix}$	$\begin{pmatrix} 0 & 0.05 \\ 0.05 & 0 \end{pmatrix} + \begin{pmatrix} 0 & 0 \\ 0.1 & 0 \end{pmatrix}$

SCYS considerations we have chosen two conditions to represent LT (in field E) and HT conditions (in field H). Textures are insensitive to variations within field H or fields B, C, D, E or F, which makes us confident that simulations are valid even if the c.r.s.s. are slightly in error.

Some comments on c.r.s.s. ratio values in Table 2 are in order. LT values include r^+ and f^+, but with a high c.r.s.s. r^+ is not part of the SCYS and the activity of f^+ is negligible. At HT we have two models: (a) does not include f^+; (b) includes f^+, which has the effect of reducing the activity of e twinning. HT (b) corresponds to higher temperature conditions than HT (a). HT (a) conditions were used to simulate the 300°C pure shear experiment and HT (b) to simulate the 400°C simple shear experiment.

Simulated textures for pure shear and for simple shear, using displacement gradient tensor increments shown in Table 3, are very different both at LT and at HT. This is first expressed in the symmetry and can already be seen on pole figures. The relationship can be described very roughly as a rotation of the texture against the sense of shear by the shear angle. But there are also distortions of the texture which result in monoclinic symmetry in the case of simple shear.

COMPARISON OF EXPERIMENTAL AND SIMULATED TEXTURES

In the previous sections we have introduced pole figures and CODs which characterize experimentally deformed limestones and calcite polycrystals subjected to a simulated deformation. Figures 5–8 document similarities and differences between corresponding patterns. The [0001] pole figures (Figs. 5 and 6) show an excellent correspondence and can be compared immediately by visual inspection. In the case of CODs (Figs. 7 and 8), patterns are much more complex and we find it useful to characterize the calcite textures by 'texture components' which represent maxima in the orientation distribution. At LT (Taylor) and 100°C (experiment), all Θ sections of the COD are dominated by a component α at $\Psi = 0°$ and $\Theta = 90°$ (Fig. 7). In the case of pure shear, the α-component is parallel to the compression direction (Fig. 7). In simple shear it is rotated away from the shear plane normal against the sense of shear (Fig. 8). Based on calculated slip activities on various systems, Takeshita *et al.* (1987) have associated this component with prevalent e twinning and r^- slip.

The HT (Taylor) and 300°C (experiment) texture is far more complex and we need several components to describe it: β and γ form a cross-like structure, while δ (at $\Psi = 90°$, $\Theta = 90°$) is parallel to the extension direction. The components are symmetrical in pure shear and rotated against the shear sense in simple shear. The β and γ components develop when all slip systems (r, f, e) are equally active and the δ component when e twinning is reduced. δ becomes dominant as temperature increases. Comparing these components (orientation maxima), we find a good correspondence between experiments and simulations even though there are differences in relative intensities of the peaks and also in minor features of the patterns. These differences can be attributed to rather special aspects of techniques and boundary conditions which we will discuss briefly in the following paragraphs. We will explore sample heterogeneity, errors in pole figure measurements, ambiguities due to pole figure inversion, and uncertainty of c.r.s.s. values in Taylor calculations or general applicability of the Taylor model.

Samples deformed in the triaxial apparatus (Kern 1977) are inherently heterogeneous, particularly in pure shear geometry. Pole figures constructed from X-ray reflection scans of the central portion of the 2 × 2 cm specimen display about 20% higher peak intensities than neutron diffraction pole figures which average over a cubic volume of 1 × 1 × 1 cm. This heterogeneity is mainly due to a strain gradient (strains near the pistons are reduced) and to a much lesser extent to minor shear bands which develop from the sample corners. The sample heterogeneity is a minor problem with respect to the general texture pattern, but it accounts for the relatively high errors in ODF calculations if neutron and X-ray pole figures are combined (Table 1).

Pole figure measurements by X-ray diffraction are subject to errors introduced by empirical intensity corrections and a blind region due to a defocusing effect which makes normalization difficult. The establishment of meaningful error criteria has become a major concern of quantitative texture analysis. One minimal requirement is that in a single pole figure with more than one symmetrically equivalent pole $\{hkl\}$ the density distribution is geometrically possible, i.e. that crystallographic constraints and correlations are satisfied. This is best analyzed by comparing experimental pole figures with pole figures recalculated from the ODF. Matthies & Wenk (1987) have determined that for perfect pole

figures the error is 1–2% (mainly due to the discretization and to rounding errors) and for good real pole figures it is 2–5%. If errors are larger than 15%, pole figures should not be used or should be remeasured (compare Table 1).

Ambiguities arise in the *pole figure inversion*; one uncertainty is introduced by the resolution of the method (about 1% for WIMV and the harmonic method). The resolution of the inversion method is illustrated by comparing observed pole figures which were not used in the inversion with calculated ones. For example, the (0006) X-ray pole figure of OS21 (Fig. 5) was difficult to measure and was not included in the ODF calculation. It shows a rather asymmetric subsidiary concentration near the center. The ODF calculated [0001] pole figure (bottom diagram in Fig. 7) shows the same subsidiary concentration; it is therefore not an experimental artifact and demonstrates resolution of pole figure measurements and of ODF calculations. Another ambiguity arises from the general indeterminability (Matthies 1979, 1982). We have estimated effects of indeterminability by expressing Taylor distributions with even and odd harmonic functions. For these particular calcite textures, the indeterminable odd contribution, which we cannot determine from pole figures without making somewhat arbitrary assumptions, ranges from −0.9 to 1.3 m.r.d. This is the maximum error which could be introduced by the inversion. Fortunately, the even and even + odd CODs show a similar pattern, and the main difference lies in peak intensities.

Another factor which causes a discrepancy between observed and simulated CODs is contained in the *Taylor model*. We are confident that our calculations were done with c.r.s.s. values corresponding to the correct major topologic domain (Fig. 10); there is less certainty about the proper subdomain, which can cause variations in the orientation distribution, particularly in the relative importance of α, β, γ and δ components (Takeshita *et al.* 1987). The δ component which increases when twinning becomes subordinate may have been underestimated in the HT(b) simple shear simulation. The assignment of a c.r.s.s. for mechanical twinning is quite arbitrary, since twins nucleate at local stress concentrations. This should be explored both experimentally and theoretically, because changes in the activity of twinning emerges as a controlling factor for texture development in calcite. We have also assumed in all calculations that the c.r.s.s. is constant during the whole deformation path and therefore have not considered dislocation work hardening or latent hardening. We also assumed that deformation was strictly homogeneous. Wenk *et al.* (1986b) have shown that for axisymmetric deformation (compression or extension) of calcite, strain can be heterogeneous; i.e. not every grain undergoes the same shape change as the whole polycrystal, and a so-called relaxed Taylor theory needs to be applied. In plane strain—at least for moderate strains—problems of heterogeneities appear to be insignificant.

In order to have direct proof of the applicability of the Taylor theory we would need to identify microstructural evidence for the activity of slip systems as a function of orientation which is extremely complicated because slip systems change along the strain trajectory. To our knowledge no such study for any material has been attempted so far and the best evidence for the applicability of a model relies with a similarity of textures. It should be noted, however, that all grains have similar aspect ratios which is consistent with homogeneous deformation. We conclude that there is overall agreement, both in pole figures and ODFs, between observed and calculated textures, and therefore our predictions of deformation textures of calcite at LT and HT, in pure shear and in simple shear are meaningful. With some confidence we can therefore also predict textures for strain paths which can, at present, not be reproduced experimentally. One important case is simple shear deformation at LT (Fig. 8). Other cases are complex strain paths discussed in the next section.

GEOLOGIC APPLICATION AND DISCUSSION

We have shown in the previous sections that calcite polycrystals deformed in plane strain develop textures which are characteristic of the strain path. Since overall agreement exists between experiments and Taylor predictions, we can use Taylor predictions to try to match the CODs of naturally deformed carbonate rocks with the simulations and obtain information about the deformation history. We choose two samples of strongly deformed marble.

The first one, OS21, is a mylonitic marble from the Palm Canyon Formation in the eastern part of the Santa Rosa mylonite zone in southern California (Erskine & Wenk 1985, Erskine 1987). Isoclinally folded marbles alternate with sillimanite schists, leucocratic gneisses and amphibolites which were deformed at upper-amphibolite grade of metamorphism. The sample is one of about 20 which have been analyzed, and appears to be representative. The pole figures and the COD are approximately orthorhombic: in the pole figures this is evident in mirror planes, in the COD it is present as a two-fold axis and an equivalence of Φ and $180° - \Phi$ sections. The COD agrees closely with Taylor predictions for low temperature where *e* twinning is the dominant mechanism and for pure shear which implies a coaxial strain path. This led Erskine & Wenk (1985) to suggest that coaxial flattening rather than shearing was the dominant mechanism for the formation of marble mylonite in Palm Canyon. The high peak maxima (4.0 m.r.d.) imply that the finite strain exceeded 30% shortening, at which level LT Taylor calculations predict that texture reaches more or less a steady-state pattern because of the compensating effects of twinning and slip.

The second sample, TV2, is a strongly lineated marble outcropping adjacent to the detachment fault of the Tanque Verde core complex in southern Arizona (Davis 1980). In contrast to the Santa Rosa sample, mirror planes are absent in pole figures. The [0001] maximum and the $[2\bar{1}\bar{1}0]$ girdle are inclined about 20° to the

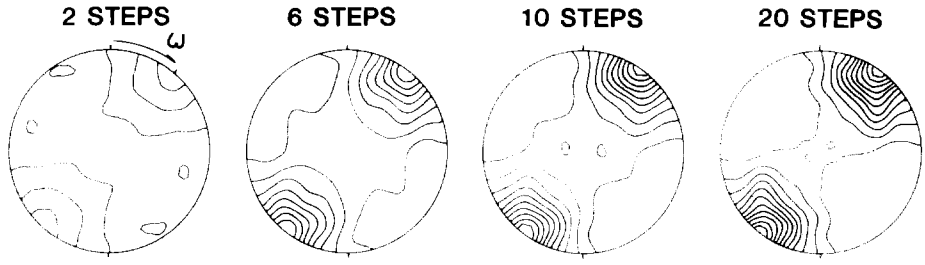

Fig. 11. [0001] pole figures for LT simple shear Taylor predictions illustrating effect of increasing strain. Note that the maximum does not rotate with increasing shear. Equal-area projection. Contour interval 0.5 m.r.d., minimum contour 0.5 m.r.d.

foliation plane. The COD still shows a two-fold axis, but Φ and $180° - \Phi$ sections are no longer equivalent. This suggests that the strain path has a significant non-coaxial component. From the displacement ω of the [0001] maximum away from the foliation plane normal (assumed shear plane) we can determine the sense of shear. In the case of the Tanque Verde sample it suggests that the top was displaced towards the SW, which agrees with geological evidence (Wust 1986).

CODs and pole figures of these natural carbonate fabrics correspond closely to LT Taylor predictions and we think therefore that similar mechanisms were active as were assumed in the predictions; i.e. *e* twinning and *r*-slip were dominant.

So far we have relied heavily on three-dimensional orientation distributions both for Taylor calculations and texture representations. Without this, conclusions would all be at the qualitative level of the symmetry concept. But having established relationships, and having identified mechanisms, we now return for simplicity to [0001]-axis pole figures to illustrate some additional features of texture development. Once a system has been thoroughly investigated a lot of information can be obtained from the more familiar pole figures and it is not necessary to calculate an ODF for every sample as long as the texture fits into a previously characterized type.

LT-Taylor calculations for simple shear document that the displacement angle of the [0001] maximum, ω, does not change with increasing deformation and is therefore independent of the shear angle (Fig. 11). The total shear is expressed in peak densities. If simple shear is combined with pure shear (Fig. 12), the displacement angle ω is smaller. It varies almost linearly with the relative amount of simple and pure shear (Fig. 13). [We define the percentage of simple shear in terms of displacement gradient tensor components as $100 \times \varepsilon_{xy}/(\varepsilon_{xx} + \varepsilon_{xy})$]. An angle of 20° indicates that 60% of the deformation occurred by simple shear and 40% by shortening.

Schmid *et al.* (1981), Dietrich & Song (1984) and Dietrich & Durney (1985) have analyzed the sense of shear from textures in limestones from thrust planes in the Helvetic nappes of the Alps. They proposed a method for estimating the simple shear component from the angle between the normal to the macroscopic cleavage and the [0001] maximum corresponding to our angle ω (Dietrich & Song 1984, fig 7). With their method, which makes different assumptions, they suggest that for 100% simple shear the [0001] maximum is inclined 45°, whereas based on Taylor calculations it is expected to be at 36° (Figs. 11 and 13).

We have so far looked at rather simple strain histories, namely pure shear (Table 3, equation 1a), simple shear (equation 1b), and a combination of the two (equation 1c). Taylor calculations can also predict texture development in more complex strain paths. We have investigated cases where pure shear (coaxial) deformation is followed by simple shear. First we assumed that the shear plane is normal to the shortening direction (Fig. 14a). Two [0001] maxima of different intensity develop. Maximum I is attributed to pure shear and weakens during simple shear deformation. Maximum II develops during simple shear and becomes dominating. We then assumed that the shear plane is inclined 45° (Fig. 14b). In this case a very strong and slightly asymmetric [0001] maximum develops at 45° to the shear plane. Notice that the influence of the original texture is still seen in intensity and pattern after an overprint of 30% strain (Fig. 11, 6 steps and Fig. 14a & b).

It is interesting to explore stress–strain behavior for

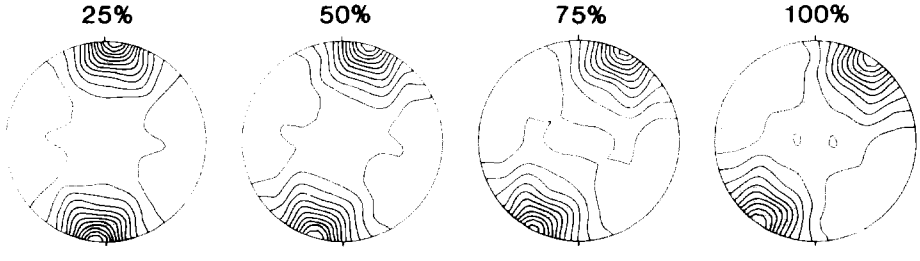

Fig. 12. [0001] pole figures of LT Taylor predictions for a displacement gradient tensor with a coaxial and a non-coaxial component (Table 3) (combination of pure and simple shear). Equal-area projection. Contour interval 0.5 m.r.d., minimum contour 0.5 m.r.d.

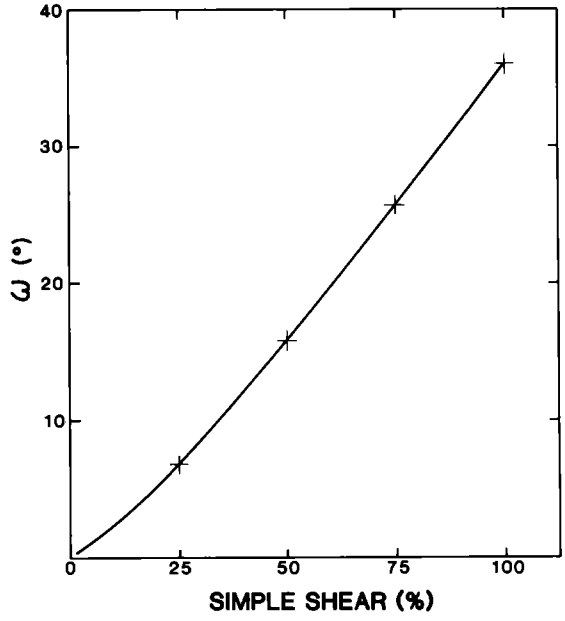

Fig. 13. Angle ω between the [0001] maximum and the pole to the shear plane (Fig. 11) for LT-Taylor predictions as a function of simple shear contribution to the deformation tensor.

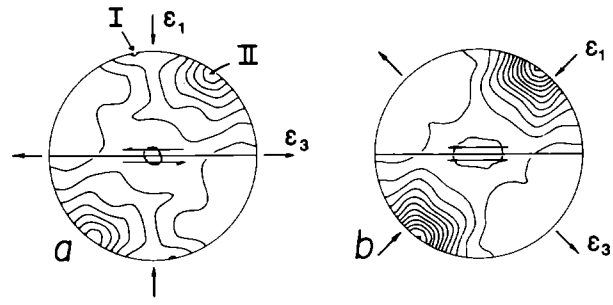

Fig. 14. [0001] pole figures for complex deformation paths in which a pure shear deformation is followed by a simple shear deformation (c.f. Fig. 15). (a) Shear plane perpendicular to ε_1 of the pure shear tensor. (b) Shear plane at 45°. Equal-area projection. Contour interval 0.5 m.r.d., minimum contour 0.5 m.r.d.

these various strain paths. An 'average stress' may be defined which is proportional to the work which is necessary to accommodate an incremental strain. The average stress is proportional to the Taylor factor which we obtain from Taylor calculations (Wenk *et al.* 1986a). Therefore we can calculate with the Taylor theory a stress–strain curve for the material which shows whether the polycrystal becomes stronger or weaker as preferred orientation develops. We wish to apply this to complex deformation paths discussed above. Unfortunately there are no reliable experimental data for stress–strain curves of calcite polycrystals deformed in plane strain, and we must rely entirely on simulations. The stress–strain curves in Fig. 15(a) predict that for pure shear, simple shear and a combination of the two, the material becomes weaker with increasing deformation. In simple shear this geometric weakening is least pronounced. For a combination of pure and simple shear the average stress is intermediate. From a work point of view, pure shear deformation is most advantageous because crystals are rotated into orientations which are most favorable for further deformation. It is therefore likely that if a unit is deformed by pure shear, continued deformation will be concentrated in the same unit rather than in adjacent, less deformed and stronger ones. This might account for the presence of strongly deformed, mylonitic carbonate bands intercalated in moderately deformed marbles in the Santa Rosa mylonite zone.

Figure 15(b) shows that if pure shear is followed by simple shear, the orientation of the shear plane is of utmost importance. If the shear plane lies in the foliation plane, crystals are in an unfavorable orientation for simple shear, and the material hardens abruptly, making this an unlikely event. By contrast, if shear planes are inclined at 45°, crystals are in a favorable orientation, and the transition from one regime to the other occurs smoothly and the resulting stress–strain curve is difficult to distinguish from that for pure shear, as is the texture. Interestingly, in all geological examples of simple shear in carbonates reported so far, shear planes are parallel to the regional foliation as defined by compositional layering. This seems to imply that deformation in shear zones such as those in the Alps described by Schmid *et al.* (1981) and Dietrich & Song (1984) started initially by simple shear, on a thrust plane and not as a secondary shear band in a homogeneously deforming sequence.

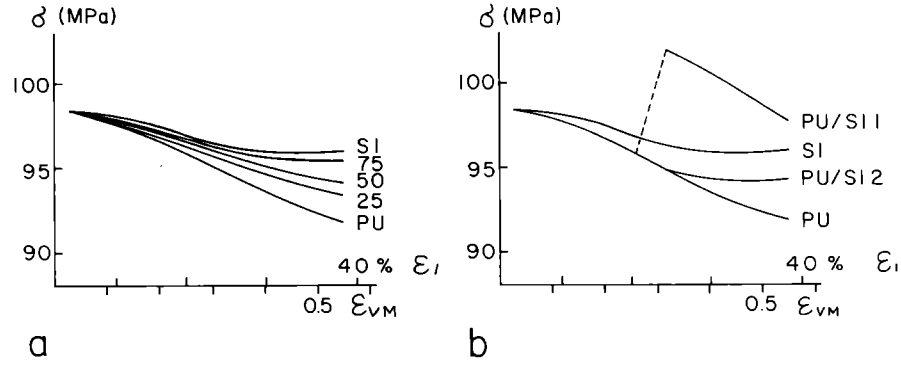

Fig. 15. Calculated stress–strain curves [mean stress (σ) vs von Mises equivalent strain ε_{VM} and the compressive strain component ε_1] illustrating hardening and weakening behavior for various strain histories. (a) Transition from pure to simple shear. (b) Pure shear followed by parallel (S11) and diagonal (S12) simple shear.

We have documented in this paper that crystallographic preferred orientation is a sensitive indicator of the strain path and allows us to distinguish between simple shear and pure shear, to determine the sense of shear, the component of simple shear and to estimate the finite strain. Taylor calculations also show that characteristic texture patterns develop for more complex strain paths such as a succession of pure and simple shear. Ultimately, of course, a previous texture pattern becomes obliterated. This depends on the specific type of texture and the strain history. As has been shown above (Fig. 14), 30% strain is not sufficient to erase a pre-existing pattern and therefore textures do not reflect the last small strain increment such as is often the case for dislocation microstructures, but a large segment of the deformation history.

Taylor calculations are specific to a particular material, and results cannot be generalized, especially not to polymineralic rocks. Nevertheless, it is noteworthy that quartzites show a similar behavior as far as the rotation of fabric patterns in simple shear is concerned (e.g. Lister & Hobbs 1980, Price 1985). Quartz also shows fabric transitions with temperature changes and textures which are much sharper compared to calcite. These transitions have been very useful in delineating isograds in deformed metamorphic belts (e.g. Hofmann 1978). One drawback is that quartz fabrics display a great variety of patterns caused by fabric transitions, strain history, often complicated by accompanying recrystallization and heterogeneous deformation (Takeshita & Wenk 1985). Natural calcite fabrics are far more monotonous, and those reported so far—within a wide range of geological temperatures, strain rates and grain sizes—all seem to belong to the LT texture type. It implies that for some reason, which needs to be further investigated, *e* twinning is more prevalent in geological situations than it is in experimental deformation. This has the advantage that we are in the large LT topology which is insensitive to minor changes in c.r.s.s. ratios, and observed fabric variations can be attributed solely to the deformation history and can therefore be interpreted with a fair degree of confidence. We propose that the methodology illustrated here should be used to investigate preferred orientation of carbonate rocks in many areas of tectonic interest. It is also essential to study experimentally the influence of the strain rate on the LT–HT fabric transition to guide us in locating natural calcite HT fabrics.

Acknowledgements—The results reported here have been collected over many years and have involved collaboration with several colleagues whose contributions are mentioned as references. We are particularly indebted to H. Kern, Kiel (for experiments); to S. Hoefler and W. Schaeffer, Jülich (for neutron diffraction pole figure measurements); and to P. Van Houtte, Louvain, A. Vadon and F. Wagner, Metz (for computer programs). We also appreciate field trips in Arizona with G. Davis and B. Smith. H.-R. Wenk acknowledges support through grants NSF EAR 84-06070 and IGPP-LANL. The thorough reviews by J. Tullis and W. Means have contributed greatly to improving the manuscript.

REFERENCES

Barber, D. J. & Wenk, H. R. 1979. On geological aspects of calcite microstructure. *Tectonophysics* **54**, 45–60.

Becker, G. F. 1904. Experiments on schistosity and slaty cleavage. *Bull. U.S. geol. Surv.* **241**, 1–34.

Bell, T. H. 1981. Foliation development—The contribution, geometry and significance of progressive, bulk, inhomogeneous shortening. *Tectonophysics* **75**, 273–296.

Berthé, D., Choukroune, P. & Jegouzo, P. 1979. Orthogneiss, mylonite and non-coaxial deformation of granites: the example of the South Armorican Shear Zone. *J. Struct. Geol.* **1**, 31–42.

Bunge, H. J. 1965. Zur Darstellung allgemeiner Texturen. *Z. Metall.* **56**, 872–874.

Davis, G. H. 1980. Structural characteristics of metamorphic core complexes, southern Arizona. *Mem. geol. Soc. Am.* **153**, 35–77.

Dietrich, D. & Durney, D. W. 1985. Change of direction of overthrust shear in the Helvetic nappes of Switzerland. *J. Struct. Geol.* **8**, 389–398.

Dietrich, D. & Song, H. 1984. Calcite fabrics in a natural shear environment; the Helvetic nappes of western Switzerland. *J. Struct. Geol.* **6**, 19–32.

Erskine, B. G. & Wenk, H.-R. 1985. Evidence for Late Cretaceous crustal thinning in the Santa Rosa Mylonite Zone, Southern California. *Geology* **13**, 274–277.

Erskine, B. G. 1987. Depositional environment and metamorphism of the Palm Canyon formation, Southern California. In: *Prebatholithic Rocks of the Peninsular Ranges Batholith* (edited by Gastil, R. G., & Miller, R.) *Mem. geol. Soc. Am.* In press.

Frost, H. J. & Ashby, M. F. 1982. *Deformation Mechanism Maps, The Plasticity and Creep of Metals and Ceramics.* Pergamon Press, Oxford.

Gil Sevillano, J., Van Houtte, P. & Aernoudt, E. 1980. Large strain work hardening and textures. *Progr. Mater. Sci.* **25**, 69–412.

Gottstein, G. & Mecking, H. 1985. Recrystallization. In: *Preferred Orientation in Deformed Metals and Rocks. An Introduction to Modern Texture Analysis* (edited by Wenk H.-R.)., Academic Press New York, 183–218.

Helming, K. & Matthies, S. 1984. On the interpretation of orientation distributions and qualitative ghost corrections for hexagonal–orthorhombic textures. *Phys. Stat. Solid.* **B126**, 43–52.

Hofmann, J. 1978. Quarzgefüge (c-Achsen Orientierung) der Metamorphite des Erzgebirges und des sächsischen Granulitgebirges als tektonische Indikatoren. *Veröff. Zent. Inst. Erdb. Forsch. Potsdam* **53**, 81–100.

Kern, H. 1977. Preferred orientation of experimentally deformed limestone marble, quartzite and rock salt at different temperatures and states of stress. *Tectonophysics* **38**, 103–120.

Kern, H. & Wenk, H.-R. 1983. Texture development in experimentally induced ductile shear zones. *Contr. Miner. Petrol.* **83**, 231–236.

Lee, J., Miller, E. L. & Sutter, J. F. 1987. Ductile strain and metamorphism in an extensional tectonic setting: a case study from the northern Snake Range, Nevada, U.S.A. *Spec. Publs. J. geol. Soc. Lond. Continental Extensional Tectonics.* In press.

Leith C. K. 1905. Rock cleavage. *Bull. U.S. Geol. Surv.* **239**, 1–216.

Lister, G. 1978. Texture transition in plastically deformed calcite rocks. In: *Proc. 5th Int. Conf. on Textures of Materials*, Vol. 2 (edited by Gottstein, G. and Lücke, K.). Springer Verlag, Heidelberg, 199–210.

Lister, G. S., Etheridge, M. A. & Symonds, P. A. 1986. Detachment faulting and the evolution of passive continental margins. *Geology* **14**, 246–250.

Lister, G. S. & Hobbs, B. E. 1980. The simulation of fabric development during plastic deformation and its application to quartzite fabric transitions. *J. Struct. Geol.* **1**, 99–115.

Lister, G. S. & Snoke, A. W. 1984. *S–C* mylonites. *J. Struct. Geol.* **6**, 617–638.

Lister, G. S. & Williams, P. F. 1979. Fabric development in shear zones: theoretical controls and observed phenomena. *J. Struct. Geol.* **3**, 283–297.

Matthies, S. 1979. On the reproducibility of the orientation distribution function of texture samples from pole figures (ghost phenomena). *Phys. Status Solid.* **B92**, 135–138.

Matthies, S. 1982. *Aktuelle Probleme der Texturanalyse.* Rossendorf-Dresden, Akad. Wiss., D. D. R., Zentralinstitut für Kernforschung.

Matthies, S. & Vinel, G. W. 1982. On the reproduction of the orientation distribution function of texturized samples from reduced pole figures using the conception of a conditional ghost correction. *Phys. Status Solid.* **B112**, 111–120.

Matthies, S. & Wenk, H.-R. 1987. Some basic requirements in quantitative texture analysis. *J. appl. Cryst.* In press.

Paterson, M. S. & Weiss, L. E. 1961. Symmetry concepts in the structural analysis of deformed rocks. *Bull. geol. Soc. Am.* **72**, 841–882.

Price, G. P. 1985. Preferred orientations in quartzites. In: *Preferred Orientation in Deformed Metals and Rocks. An Introduction to Modern Texture Analysis* (edited by Wenk, H.-R.). Academic Press, Orlando, Florida, 385–406.

Rehrig, W. A. & Reynolds, S. J. 1980. Geologic and geochronologic reconnaissance of a northwest trending zone of metamorphic core complexes in southern and western Arizona. In: *Cordilleran Metamorphic Core Complexes* (edited by Crittenden, M. D., Jr., Coney, P. J. & Davis, G. H.). *Mem. geol. Soc. Am.* **153**, 131–157.

Roe, R. J. 1965. Description of crystallite orientation in polycrystalline materials. II. General solution to pole figure inversion. *J. appl. Phys.* **36**, 2024–2031.

Schmid, S. M., Casey, M. & Starkey, J. 1981. The microfabric of calcite tectonites from the Helvetic nappes (Swiss Alps). In: *Thrust and Nappe Tectonics* (edited by McClay. K & Price, N. J.). *Spec. Publs geol. Soc. Lond.* **9**, 151–158.

Simpson, C. 1984. Borrego Springs–Santa Rosa mylonite zone: a Late Cretaceous west-directed thrust in southern California. *Geology* **12**, 8–11.

Takeshita, T., Tomé, C. N., Wenk, H.-R. & Kocks, U. F. 1987. The single crystal yield surface of calcite polycrystals and texture transitions. *J. geophys. Res.* In press.

Takeshita, T. & Wenk, H.-R. 1985. The effect of geometrical softening on heterogeneous plastic deformation in quartzites. *EOS, Trans. Am. geophys. Un.* **66**, 1085.

Tullis, J., Christie, J. M. & Griggs, D. T. 1973. Microstructures and preferred orientations of experimentally deformed quartzites. *Bull. geol. Soc. Am.* **84**, 297–314.

Van Houtte, P. & Wagner, F. 1985. Development of textures by slip and twinning. In: *Preferred Orientation in Deformed Metals and Rocks. An Introduction to Modern Texture Analysis* (edited by Wenk, H.-R.). Academic Press, Orlando, Florida, 233–258.

Wagner, F., Wenk, H.-R., Esling, C. & Bunge, H. J. 1981. Importance of odd coefficients in texture calculation for trigonal–triclinic symmetries. *Phys. Status Solid.* **A67**, 269–285.

Wagner, F., Wenk, H.-R., Kern, H., Van Houtte, P. & Esling C. 1982. Development of preferred orientation in plane strain deformed limestone. Experiment and theory. *Contr. Miner. Petrol.* **80**, 132–139.

Wagner, F., Wenk, H.-R., Kern, H. & Van Houtte, P. 1984. Evolution of deformation textures in calcite. *Proceedings Seventh Int. Conf. on Textures of Materials, Zwijndrecht, Holland*, 165–171.

Wenk, H.-R. (Ed.). 1985. *Preferred Orientation in Deformed Metals and Rocks. An Introduction to Modern Texture Analysis*. Academic Press, Orlando, Florida.

Wenk, H.-R. & Kocks, U. F. 1987. The representation of orientation distributions. *Metall. Trans.* **18A**, 1083–1092.

Wenk, H.-R., O'Brien, D. & You, Z. 1985. Spherical representation of orientation distribution functions. *Phys. Status Solid.* **A90**, K19.

Wenk, H.-R., Takeshita, T., Van Houtte, P. & Wagner, F. 1986a. Yield strength and texture development of calcite polycrystals, *J. geophys. Res.* **91**, 3861–3869.

Wenk, H.-R., Kern, H., Van Houtte, P. & Wagner, F. 1986b. Heterogeneous strain in axial deformation of limestone, textural evidence. *Am. Geophys. Un. Monogr.* **36**, 287–295.

Wenk, H.-R., Kern, H. & Wagner, F. 1981. Texture development in experimentally deformed limestones. In: *Deformation of Polycrystals: Mechanisms and Microstructures, Proc. 2nd Riso International Symposium on Metallurgy and Materials Science*, 235–245.

Wust, S. 1986. Regional correlation of extension directions in Cordilleran metamorphic core complexes. *Geology* **14**, 828–830.